

Kenneth E. Perry<sup>1</sup>, Matthew M. Quest<sup>2</sup>, Tim J. Johnson<sup>2</sup>, Robert Conta<sup>2</sup>

## In Vivo Strain Estimates for Medical Implants

---

*Anticipating the in vivo loading conditions is a challenging aspect of validating the design and durability of cardiovascular implants. Complex implant geometries, multi-axial displacements, device/tissue interactions and time dependent factors can make it difficult or impossible to identify a single loading cycle that is representative of the full range of conditions. Computational modeling is often used to reduce a large number of complex conditions into representative alternating and mean strains at locations of maximum strain. A novel approach for estimating the alternating and mean strains during in vivo loading will be presented. The method determines local strains by deforming a finite element model of an implant into a three dimensional geometry reconstructed from two dimensional images of a physically deformed implant. The method is then extended to in vitro fatigue experiments. Two examples are given of a structural heart implant.*

**KEY WORDS:** *Computational models, experimental mechanics, inverse methods, medical devices, imaging, Nitinol*

### Introduction

During the design verification and validation process, in vitro tests are used to determine whether a medical device performs according to specifications and to help predict in vivo performance. Many medical devices undergo cyclic loading throughout their lifecycle; thus, fatigue testing is an important component of verification testing. Regardless of the fatigue test paradigm being followed (test-to-success or test-to-fracture), it is necessary to characterize, parameterize and bound the anticipated cyclic loading for use in durability specifications.

The fatigue performance of deformable structures is directly related to the deformation and motion amplitudes the structures experience. Therefore, determining the physiologic conditions that a cardiac implant encounters in the body is critical to device lifetime prediction and demonstration. Results from fatigue tests are typically used in statistical models, and therefore the test conditions must be precise, well-defined and controllable to minimize the variability in test results. Ideally, test conditions should be developed from well known, precise and representative measures of the in vivo conditions.

However, acquisition of representative in vivo data can be difficult for medical devices that are unique or placed in novel areas of the body. This is particularly true for cardiac implants placed in locations where the dynamic properties of the surrounding anatomy are not well known, cannot be measured directly, and can be altered by a device in situ. Static deformations can be directly measured in an animal model (e.g. after sacrifice), but it is challenging to map the motions associated with a device in a beating heart. In addition,

---

<sup>1</sup>ECHOBIO LLC, 566 Stetson Place, Bainbridge Island, WA 98110

<sup>2</sup>Cardiac Dimensions, Inc., 5540 Lake Washington Blvd. NE, Kirkland, WA 98033

animal models do not always accurately represent the conditions found in comparable human anatomy. The amount of deformation or motion can be substantially different in healthy animals versus sick patients, because healthy tissue can interact differently with an implanted device. Measurements are further confounded by the potential for the measurement method itself to interact with the device or tissue and reduce the fidelity of the measurement.

Preferably, a non-contacting, non-invasive measurement method should be used for measuring deformation and motion of a medical device in situ. Ideally, the data from this non-contacting method should be incorporated into the durability test development as early as possible. Advances in medical imaging and computational methods have made CT, MRI and radiography powerful tools for investigating three-dimensional motion and deformation [1], but the data must be further processed to create quantitative parameters for use in durability tests.

We have developed a technique that allows quantitative analysis of both in vivo and in vitro conditions with a single method. It is based on biplane cinefluoroscopy and allows virtual reconstruction of an implanted medical device, thereby allowing precise quantitative measurements of in vivo deformations and motions. These measurements may then be used to reduce the number of parameters used for rigorous in vitro fatigue tests. Finally, the reconstruction method used for in vivo conditions may also be used to reconstruct in vitro devices. Both in vitro and in vivo computations can then be compared and contrasted to verify the assumptions and simplifications that were required to reduce the complex, multivariate in vivo conditions to those suitable for a fatigue test. Fatigue results may be directly linked to in vivo conditions because equivalent computational methods can be used for both.

## Methods and Materials

### *Cardiac Implant*

The XE2<sup>TM</sup> implant of the CARILLON<sup>®</sup> Mitral Contour System<sup>®</sup> (Cardiac Dimensions, Kirkland WA, USA) has been evaluated in the TITAN clinical study [2]. The XE2 has been developed to treat functional mitral regurgitation and is delivered percutaneously through a 9Fr catheter to the Coronary Sinus (CS) and Great Cardiac Vein (GCV). The distal end of the implant is deployed and anchored within the GCV, proximal traction is applied to reshape the mitral annulus and then the proximal end of the implant is deployed and anchored into the CS.

The XE2 implant is manufactured with superelastic NiTi wires. The flexible NiTi wires that form the endoluminal anchors deform during deployment to exert anchoring force against the CS/GCV lumen. The wires then move as the heart beats. See Figure 1.

### *In Vivo Imaging*

Cinefluoroscopy provides excellent spatiotemporal resolution throughout the cardiac cycle. The pixel size of cinefluoroscopic images is often smaller than 0.2mm. In addition, the 15 to 30 frames/second frame rate of cinefluoroscopy provides an accurate radiographic snapshot without the motion artifacts that may cause blurring and reduced resolution in CT. Therefore, cinefluoroscopy is a valuable platform for measuring minute displacements of small structures, particularly in applications wherein the structures of interest are moving

rapidly (e.g. a cardiac implant moving during the cardiac cycle). However, single-plane cinefluoroscopy is limited in application due to inaccuracies associated with view dependent parallax and cosine errors that can be present.

Synchronous Biplane Cinefluoroscopy (SBC) is an imaging modality that can reduce the parallax and cosine errors inherent in single-plane fluoroscopic images. SBC imaging systems acquire single-plane cinefluoroscopic images from two distinct directional views with individual frames that are captured at nearly the same time. By analyzing the geometric information from both views, the geometry of the implant can be resolved in 3D and foreshortening errors eliminated. Combined with the better spatiotemporal resolution of cine, SBC provides a precise method for resolving small displacements (e.g. under 2mm) and structures (e.g. stent struts or small diameter wires).

Imaging data of the implanted device was collected from multiple fluoroscopes at various European clinical sites used in the clinical evaluation of the XE2 implant. SolidWorks (Dassault Systmes S.A., Vlizy, France), a 3D solid modeling (CAD) program, was used to perform the post processing of SBC image data to reconstruct virtual devices using the method described in the Biplane Reconstruction section below.

### *Biplane Reconstruction*

First, each analyzed SBC frame in a given DICOM image dataset was exported as separate left and right images that could be individually imported into CAD, see Figure 2. CAD models were then created for each analyzed frame using following procedure. Planes for each of the SBC images were created utilizing the image orientation information embedded in the DICOM dataset (see Figure 3). Typically, the two images were captured from approximately  $60^\circ$  LAO/ $-15^\circ$  Caudal and  $-30^\circ$  RAO/ $-15^\circ$  Caudal, but the image projections varied and images from any two projections may be utilized.

Reference lines were placed on both the left and right image planes, again using the orientation data from the DICOM dataset, to allow the images to be rotated to compensate for rotation of the fluoroscopic imager (as shown in Figure 3).

The two images were then placed on the appropriate plane and aligned with the appropriate reference line. To ensure that the two images were scaled and vertically aligned with one another, a series of horizontal lines were constructed using reference features on the implant in one of the images, while the other image was scaled and moved vertically until all of the reference features were aligned. Vertical alignment is critical to ensure that features intersect when projected into 3D space. However, horizontal alignment is unimportant due to the way the planes are aligned in CAD; horizontal displacement of an image only changes the position of the resulting geometry in 3D space and does not affect the shape. Typically, between four and five reference features were utilized for each frame to ensure that only one image scaling and alignment solution existed.

Once the images were properly scaled and aligned to each other, two non-deformable components on either end of the implant were reconstructed and their lengths measured in pixels. These measured lengths were later used to scale deformation measurements taken in the resulting 3D CAD model from pixels to inches. The non-deformable components were reconstructed by first sketching their axes on the left and right images. These 2D axes were then projected normal to their respective sketch planes creating surfaces. Lines were created at the intersections of these surfaces to form the component axes in 3D space. See Figure 4.

The lengths of the two lines were then measured in the reconstructed CAD model.

Once the rigid component lengths were measured, other non-deformable features were reconstructed through radiometric scaling in CAD and compared to the original cine image. For example, the unscaled diameter of the rigid components in pixels could be determined by multiplying the measured length in pixels by the known ratio of diameter to length in inches. This enabled a qualitative confirmation for how well the reconstructed model fit the imaging dataset.

Deformable implant features (e.g. the anchor wires) were also reconstructed using this methodology. After all relevant features had been reconstructed, coordinate system origins were placed on and aligned to the non-deformable components. Measurements in pixels were taken from these origins to fiducial features placed on the deformable implant components.

While the above procedure is described sequentially, it was an iterative process. A complete cardiac cycle typically consisted of 12 to 15 cine frames. Initially, only three to five frames were analyzed with the left to right image scaling and frame scale factors derived from the two rigid components evaluated for each frame. The image scaling was then adjusted slightly until a single image scaling factor was identified that provided a good fit across all frames. Once the image scale factor was identified, additional frames were analyzed.

Following the creation and analysis of all of the CAD models for a patient dataset, deformation measurement scaling from pixels to inches was completed using Excel (Microsoft, Redmond, WA, USA). A device scale was determined by dividing the non-deformable component lengths by their known lengths. Each of the unscaled measurements in pixels was then converted into a scaled inch measurement by multiplying the unscaled value by the device scale.

Checks and verifications were performed to ensure the reconstructed model accurately represented the in vivo condition. Multiple reference features were used to align the left and right images. These same features were used successfully across multiple frames in each dataset. A single image scaling factor was identified for each DICOM dataset. In addition, the frame scale factors derived from the length of the two rigid components were independently determined across frames and matched closely (to within 3%). The reconstructed model compared favorably to images of deformed implants. Finally, the overall length of the implant was measured in the reconstructed model and, in all cases, the measured value was within the design specification for this dimension. Taken together, all of these factors indicate that the resulting reconstructions are accurate representations of the deformations imposed by the in vivo environment.

## Finite Element Models

A global finite element model was created for the proximal anchor of the XE2 implant in a relaxed state using a coarse mesh of linear elements and is shown in Figure 5. The mesh was constructed by extruding twelve elements defined in the cross section the full length of the wireform. The global consisted of over 12,000 8-noded brick (C3D8) elements with approximately 1,000 nodes along the centerline and a spacing of about 0.15 mm.

A coarse mesh was used for the global model to avoid overconstraint and convergence issues and also to increase computational efficiency and solution speed. Mesh density and other model studies were performed to optimize the choice of node spacing along the centerline of the global model and the mesh density through the cross section of the wire.

Continuum, three-dimensional elements were chosen for the global model over beam elements because these more simple element formulations lack adequate contact capabilities. The XE2 proximal anchor has several regions such as the apical twist that involve self contact and/or contact with other portions of the implant. It was found that these interactions played a significant role in the reponse of the XE2 and needed to be included in the model.

A sub-model approach was adopted to study fatigue strain history in specific regions of interest. Figure 6 is a sub-model of the region of interest of the proximal anchor of the XE2. The submodel utilized the same model properties as the global model and provided much finer resolution for subsequent stress/strain calculations.

The submodel was coupled to the global model at cross section/planes shown in Figure 6 and constraints were also used for nodes within and in contact with other non-deformable components, represented in Figure 6 as three planes.

Linear, 8-noded bricks were again used, but for the sub-model, there were 60 elements in the cross section and over 100,000 elements for the region of interest. Fully integrated (C3D8I) elements were used and a local material coordinate system was used for fatigue post-processing.

Rigid bodies were included in both of the models to interact with the deforming wireform and represent non-deforming physical geometry. General contact was enforced throughout both the global and sub-model analyses. Material properties for the wireform and other essential aspects of the models were specified, such as boundary conditions and contact parameters, as would be typically specified.

All analyses were performed using ABAQUS/Standard 6.10 (SIMULIA Providence, Rhode Island).

### **Motion and Strain Analysis**

Analysis of measurements that were taken throughout the cardiac cycle allowed quantification of the in vivo mean and alternating deformations of the device. Mean deformations were calculated by taking the difference between the in vivo reconstruction values and measurements made from the same origins on un-deformed devices. Motion amplitudes were determined by taking the difference between the minimum and maximum deformation values. Two frames (and the correlated 3D CAD models) that corresponded to the minimum and maximum deformation conditions were chosen to use as input to the computational model. These two frames had the largest displacement of a fiducial feature at the apex of the implant, which was found in previous analyses to have the largest motion in frame-by-frame inspections across of a larger number of patients.

The parametric spacing of the tabulated coordinates for the in vivo reconstruction centerlines were adjusted by fitting tensioned splines to the raw data and interpolating at uniform increments to correspond to the centerline node locations of the global model shown in Figure 5. In general, reconstructed data was not completely available along the entire centerline of the wireform. In such cases, each segment for both frames was carefully registered and aligned to the undeformed global model in an iterative process to ensure an accurate translation.

Special attention was taken to ensure that the individual segments of the resampled curves produced results that matched the original data, especially in the region of interest. Inconsistencies, gaps, outliers or discontinuous segments were identified and either eliminated

or replaced at this step in the process. The location and curvature of the interpolated data points were carefully checked to preserve the original continuous waveform shape, particularly at free ends and where segments are joined. Consistent with previous efforts, the nominal waveform length was maintained, by using it as a fitting parameter for application to the deformed model.

## Results

### *In Vivo Reconstruction*

Implant loading conditions were created for two patients, A and B. Each set was reconstructed in CAD according to the methods described above and tabulated centerline data was used to drive the global model for the proximal anchor of the XE2. To qualitatively assess the fidelity of the computational results, the deformed finite element models were compared to the original SBC images as shown in Figure 7 for patient A. The resulting computational models produced high quality reproduction of the deformation in the region of interest.

### *Comparison of Different Patient Loading Conditions*

The virtual reconstructions and centerline data for minimum and maximum deformation (based on the relative displacement of the fiducial described above) were developed for patients A and B. The max and min deformed global model centerline nodes for each patient are shown in Figure 8.

The nodal centerlines for the max and min fatigue cycle positions are clearly distinguished in Figure 8. Gaps in the centerline data exist and were discussed above. The deformation of the proximal anchor for patient A is seen to be more symmetrical than that for patient B.

### *In Vivo Fatigue Strain Results*

Sub-models of the region of interest were run for patients A and B, and a fatigue analysis was performed to estimate the applied mean and alternating strain. Contour plots of alternating fatigue strain for the two patients are shown in Figure 9 and Figure 10 is a plot of the alternating versus the mean strain.

Even as the gross deformation for patients A and B are seen to be different, the alternating and mean fatigue strains in the region of interest have similar magnitudes and occur in generally the same locations.

### *In Vitro Reconstruction*

Reconstructions of an in vitro condition were also created using the methodology described above, but using photographs of the implant taken from two angles while on-test. A bench model similar to that used for fatigue testing the XE2 is shown in the Figure 11 (lower left). This bench model was designed to hold the proximal anchor and pull on the fiducial feature at the apex to replicate the deformations observed in the clinical images, shown in the upper left of Figure 11. The location and amplitudes of the strains compared favorably at the region of interest for both in vitro and in vivo models suggesting that the bench model provides a reasonable representation of in vivo fatigue strains.

## Discussion

Virtual reconstructions derived from precise 4D image data enable quantitative validation of the reconstruction method, computational model and strain calculations by comparing models based on in vivo and in vitro data. Since the data is quantitative, the associated uncertainty of the measurements can be measured with statistical methods to demonstrate statistically valid boundary conditions. While engineering judgment may still be required because small, practicable sample sizes will have large confidence intervals, the accuracy of the underlying cyclic loads can be greatly improved. Additionally, quantitative data can be applied directly to empirical tests or used in computational models. For imaging modalities that allow observation in 3D, fiducial features may be identified and the motion of those features evaluated. This evaluation can be used to reduce the number of parameters to those that are considered important and to create a physiologic envelope that bounds multiple axes of motion.

With FEA based on clinical imaging data, computational models become more independent tools for use in both validation and prediction. The fatigue model does not need to rely on boundary condition inputs that may not be relevant to the design or conditions. Portions of a device may be analyzed using inputs derived from known clinical conditions and the calculated strains can be calibrated with test-to-fracture results from fatigue conditions near those observed in vivo. Gaps may exist in the clinical imaging data where the high strain locations are hidden or too small to acquire precise estimates. These gaps are not critical because computational models that utilize a fully reconstructed 3D model as input may rely on extrapolation from remote locations where the conditions are well known. Sensitivity analyses may be used to validate and revalidate the assumptions made when the number of parameters is reduced to apply the conditions on test, and the limits may be derived from a 3D envelope of conditions for a small sub-model or portion of the device.

Furthermore, the calculated strains can be validated by deforming a device in vitro, measuring the strains on the device with an alternate method (e.g. strain gages, digital image correlation, etc.), photographing the silhouette of the deformed device from two views, reconstructing the deformation and motion, and then comparing the strains calculated in the computational model to those measured in the physical device using the alternate method. The deformations for the in vitro test are selected to be qualitatively similar to that observed in vivo, so the measured strains are anticipated to have strong correlation to the computed values. Because the same methodology can be used for in vitro and in vivo strain calculations, the model derives consistent strain measures for both environments that can be correlated.

The methodology was demonstrated above by using geometry derived from SBC in computational models of a cardiac implant to calculate in vivo mean and alternating strains. The technique can potentially add freedom to the design and evaluation of implantable structures. For example, worst case conditions can be estimated from statistical models of reconstructed image data, applied in fatigue tests, and then validated through the computational model in a more traditional fashion. Statistical models of both the fatigue strength and physiologic conditions can be decoupled, refined independently, and then recombined to estimate the probability of fatigue fracture, resulting in a quantitative measure of risk.

By decoupling the analysis of the physiologic loading conditions from the fatigue strength (the two are coupled in a test-to-success), the device design may be incrementally improved by decreasing the alternating strains where fractures occur in the test-to-fracture and then

comparing the result to models of the physiologic conditions that have increasing confidence. The design modifications should be limited to relatively small spatial regions of high strain because the transfer function between motion and alternating strain will be correlated to the interaction between the global device geometry and the anatomy.

## Conclusion

A single methodology can be used to effectively compute strains for a device in vitro and in vivo. Quantitative 3D reconstructed models can be built from two viewing angles. The 3D reconstructions provide spatial data that can be applied directly in a fatigue test, without requiring a computational model to derive the conditions. The definition of the in vivo physiologic envelope allows early determination of an empirical fatigue strength design margin. This method can confirm that the simplifications applied early in the durability test development are appropriate, enabling early test-to-fracture along the most common or largest axes of motion for the device.

The use of high-resolution 4D imaging emphasizes the need for clinical data as early as possible for use in the design and development of high reliability medical devices. As more clinical data is collected, a statistical model of the physiologic parameters can be refined independently of the device and the risk-profile updated accordingly.

High resolution finite element models, combined with in vivo imaging and their associated measurements, aid in understanding the boundary conditions of relevant fatigue parameters. The computational models based on reconstructions (in vivo and in vitro) allow direct comparison of in vivo and in vitro mean and alternating strains, potentially shortening design cycles and improving the value of in vitro tests for medical devices.

## References

- [1] C.A. Taylor and C.A. Figueroa. Patient-specific modeling of cardiovascular mechanics. *Annu Rev Biomed Eng*, 11(4):109–34, 2009.
- [2] T. Siminiak, J.C. Wu, M. Haude, U.C. Hoppe, J. Sadowski, J. Lipiecki, J. Fajadet, A.M. Shah, T. Feldman, D.M. Kaye, S.L. Goldberg, W.C. Levy, S.D. Solomon, and D.G. Reuter. Treatment of functional mitral regurgitation by percutaneous annuloplasty: results of the TITAN trial. *Eur J Heart Fail*, 14(8):931–938, 2012.

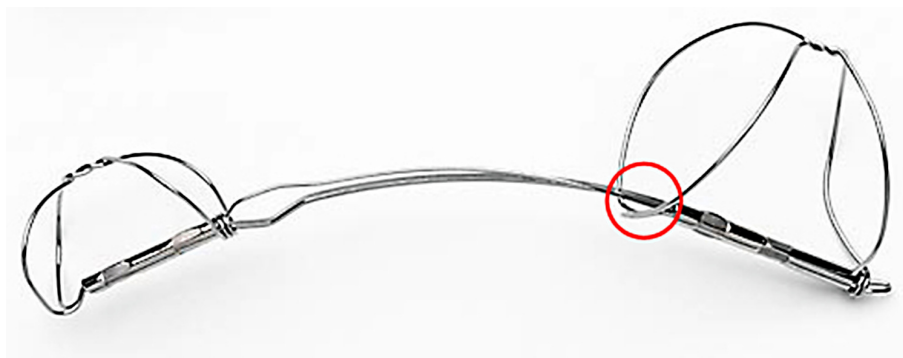


Figure 1: The CARILLON Mitral Contour System XE2 implant. The proximal end of the implant is shown on the right with the region of interest evaluated in this paper circled.

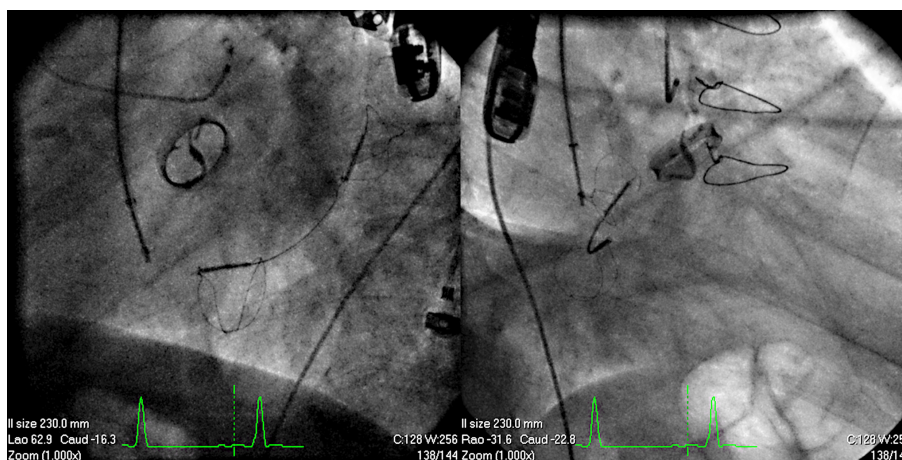


Figure 2: A representative SBC frame showing the synchronized left and right images. Note the image orientation embedded in the lower left of each image.

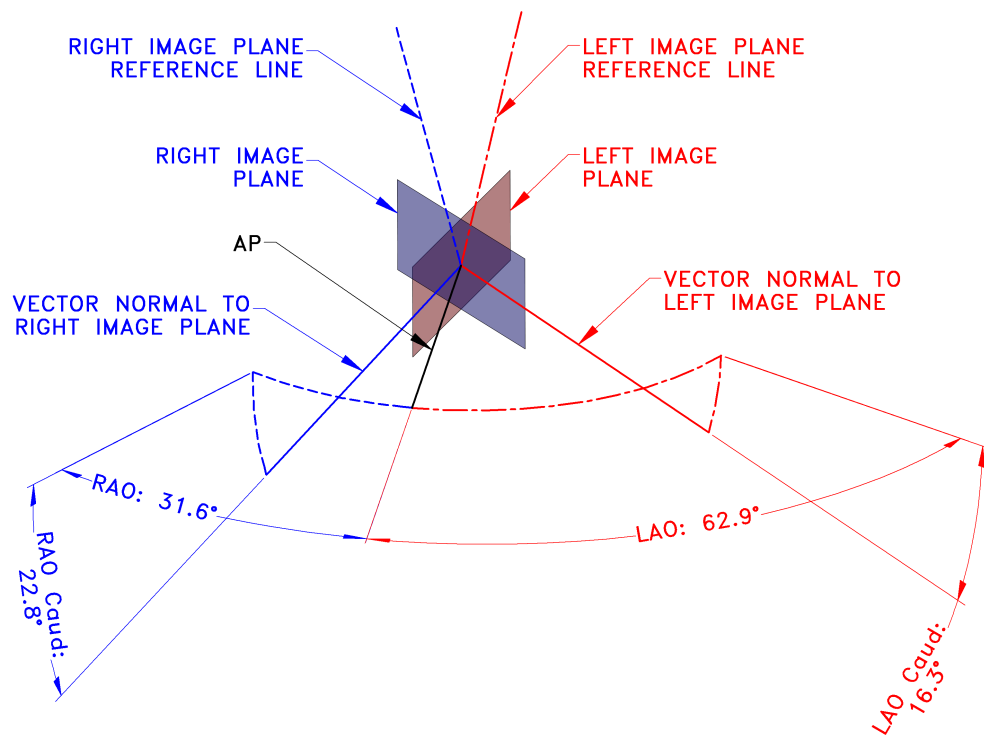


Figure 3: Setup of SBC image planes in CAD. The angles used to setup the planes are taken from the left and right images and are relative to the AP direction. Reference lines placed in the left and right image planes are used to orient the images.

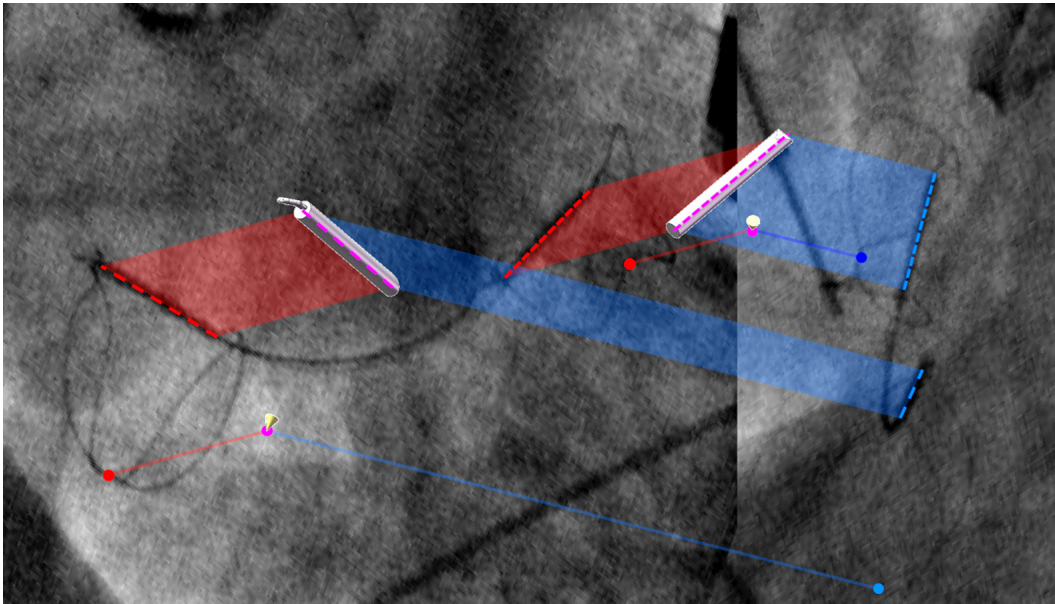


Figure 4: A typical reconstruction showing the two non-deformable components (silver cylinders) used to scale the resulting CAD model. The feature axes are shown on the left (red lines) and right (blue lines) images; the resulting 3D axes are shown in purple. Also shown are the two fiducial points at the apex of the implant that were used for deformation measurements

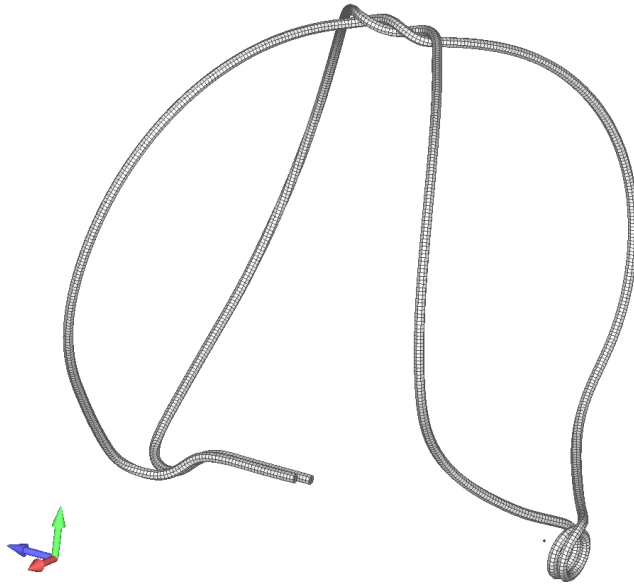


Figure 5: Finite element global model used to link the reconstructed displacements and the deformation of the XE2.

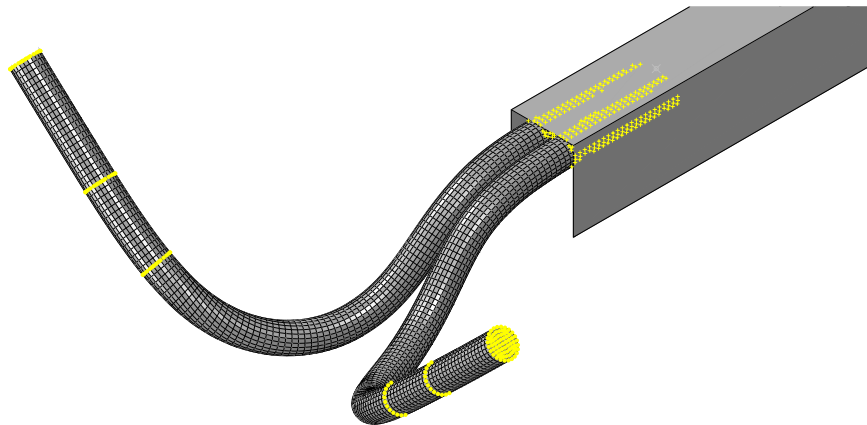


Figure 6: Finite element sub-model of the region of interest on the proximal anchor of the XE2.

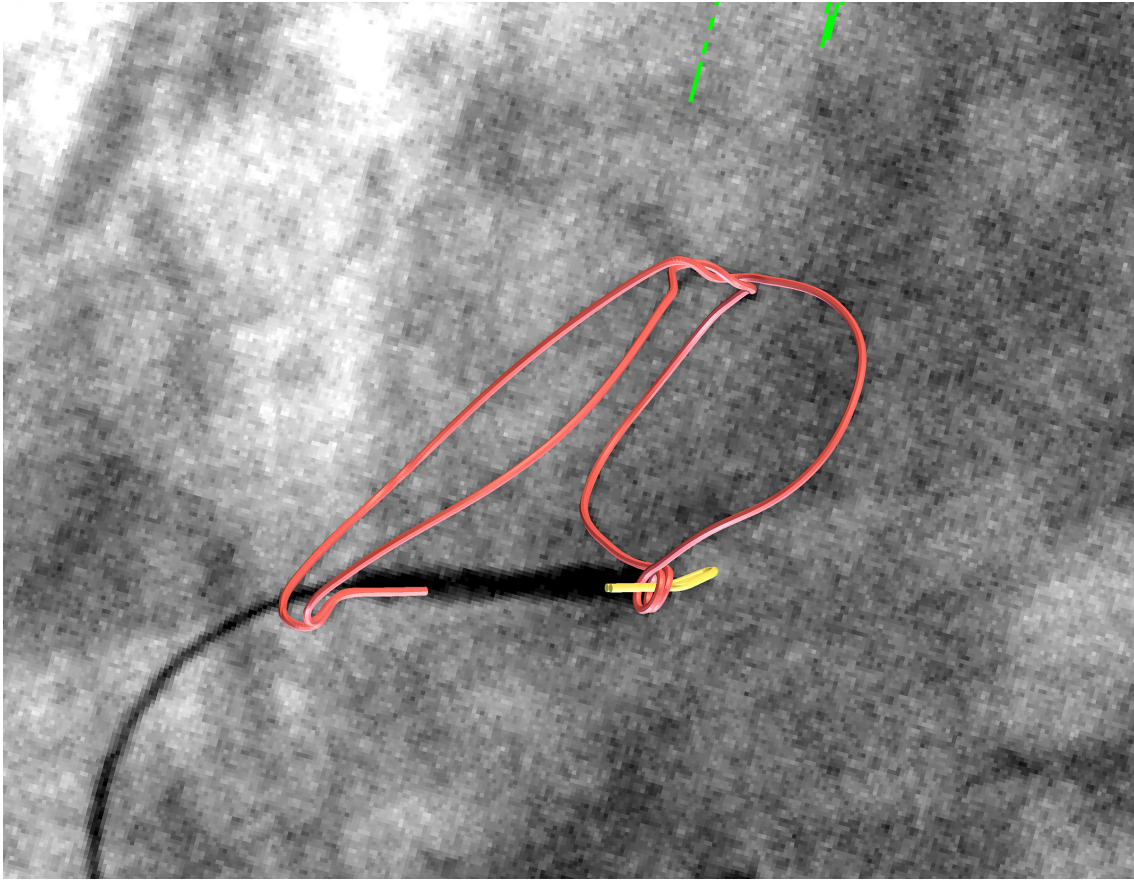


Figure 7: Comparison of the deformed FEA model to the original cine frame for patient A. The deformable NiTi proximal anchor wireform is shown in red and a non-deformable ratiometrically scaled feature is shown in yellow.

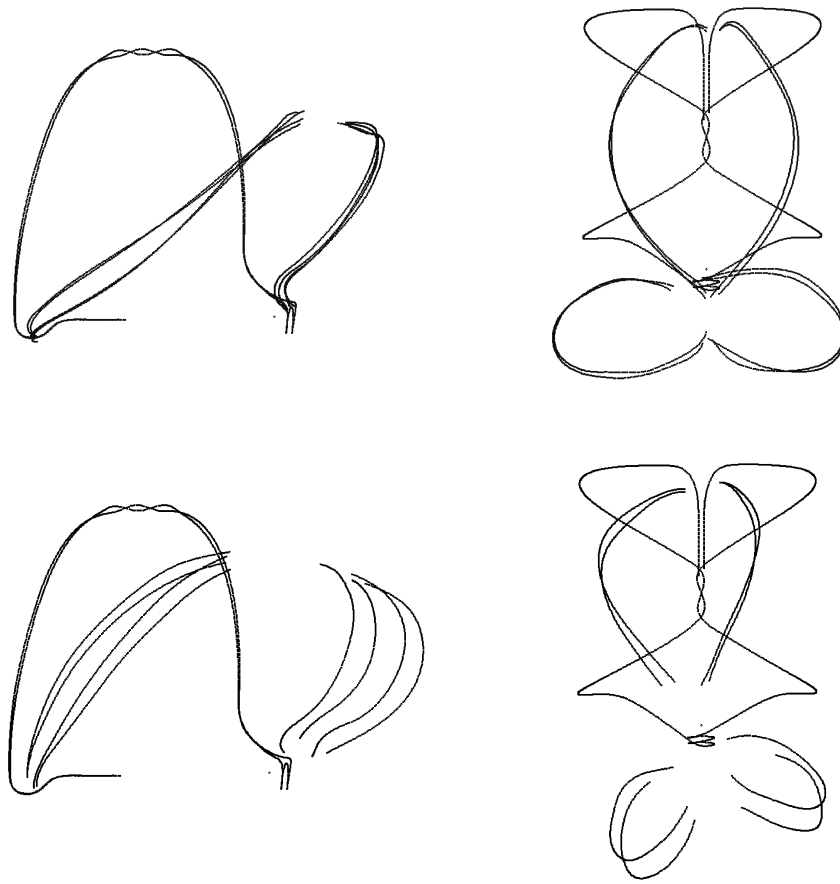


Figure 8: Comparison of in vivo deformations for patients A (top) and B (bottom).

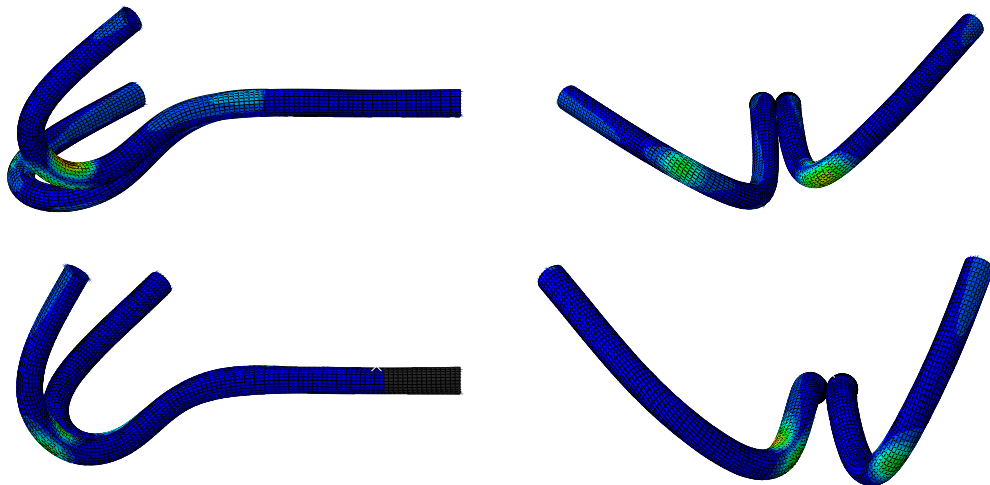


Figure 9: Contour plots of alternating fatigue strain for patients A (top) and B (bottom).

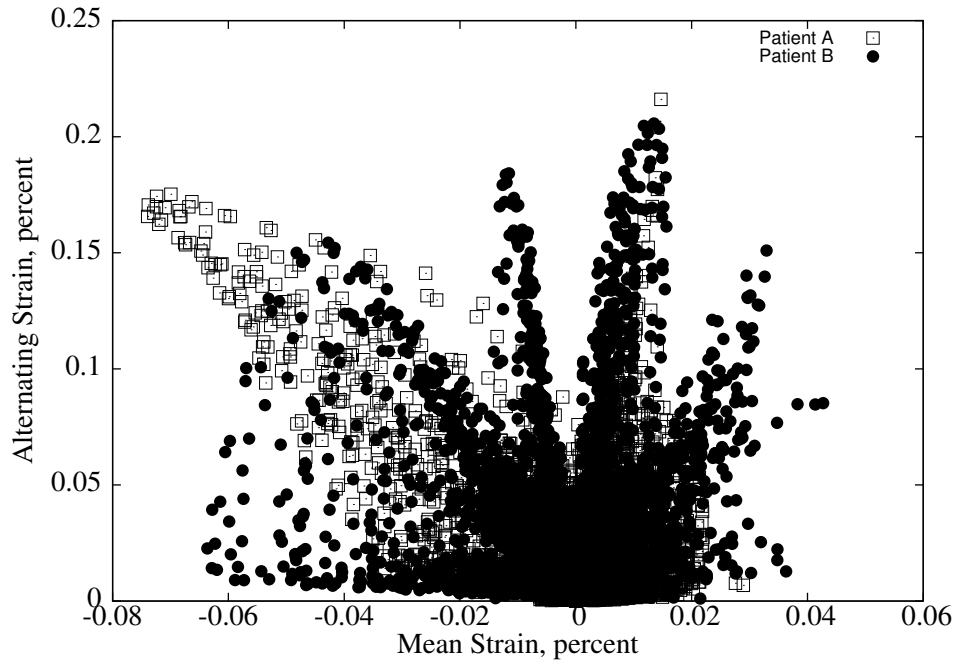


Figure 10: Alternating versus mean strain for patients A and B.

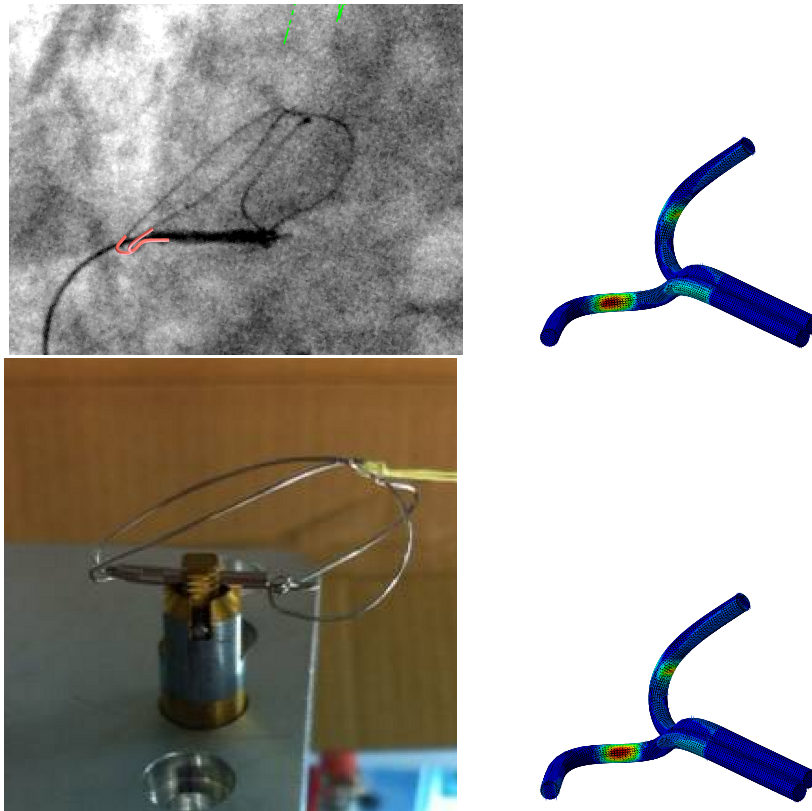


Figure 11: Deformation and alternating fatigue strain results for simulations of in vivo (top) and in vitro (bottom) loading of the XE2.